Baseline Decorrelation in Bistatic Interferometric SAR Systems Over Bare Soil Surfaces

Gerardo Di Martino, *Senior Member, IEEE*, Alessio Di Simone, *Member, IEEE*, Antonio Iodice, *Senior Member, IEEE*, Daniele Riccio, *Fellow, IEEE*, and Giuseppe Ruello, *Senior Member, IEEE*

***Abstract*— In the context of bistatic synthetic aperture radar (SAR) imaging, SAR interferometry is an appealing application due to the capability of retrieving accurate topographic information or surface deformations at fractions of wavelength. Within this framework, we present a new physical-based approach to evaluate the correlation between a pair of bistatic SAR acquisitions over a bare soil surface and in a very general imaging geometry, which includes two transmitters and two receivers. Some specific configurations of practical interest for proposed bistatic spaceborne SAR missions, for example, SESAME and PLATiNO-1 (PLT-1), namely coplanar and along-track bistatic geometries, are analyzed as well. The proposed methodology makes use of electromagnetic scattering models suited to random rough surfaces, namely the Kirchhoff approximation (KA) and the first-order small-slope approximation (SSA1), under which analytical formulations of the correlation between the received electromagnetic fields are derived. It is found that in the coplanar imaging geometry, a unitary correlation coefficient can be obtained with nonnull orthogonal baselines. Closed-form expressions of the critical baseline are derived as well. The proposed approach can be applied to such scenarios where single surface scattering is the dominant mechanism, such as bare soil surfaces or scarcely to moderately vegetated areas.**

***Index Terms*— Bistatic radar, coherence, synthetic aperture radar (SAR) interferometry.**

I. Introduction

SYNTHETIC aperture radar (SAR) interferometry is a well-known technique able to retrieve accurate terrain topography [1], [2] or small terrain movements [3], [4], [5] from the proper combination of multiple acquisitions. The most common implementation of the technique consists in the combination of monostatic SAR images acquired at different times (repeat-pass interferometry) [1], [2], [3], [4], [5], which is necessary for terrain movement retrieval, but often employed also for topographic applications. More accurate topography measurements are obtained by using a transmitting-and-receiving antenna and an additional receiving-only antenna (single-pass interferometry) [6], [7], that is, by combining a monostatic SAR acquisition with a bistatic one. If the two antennas are carried by a single platform, as in the Shuttle Radar Topography Mission (SRTM) [6], the SAR interferometry system is usually considered to be monostatic. Conversely, if the two antennas are carried by different platforms, as in TanDEM-X [7], the SAR interferometry system is usually considered to be bistatic. However, conceptually the two implementations are identical, and here we will refer to them as single-pass monostatic SAR interferometry.

Recently, fully bistatic implementations have been proposed [8], [9] and experimentally implemented [9], which imply the use of one transmitting-only antenna and two closely spaced receiving-only antennas. In this case, both the SAR acquisitions of the interferometric pair are bistatic, and here, we will refer to this implementation as single-pass bistatic SAR interferometry. Moreover, bistatic SAR experiments are being currently performed [10], thus paving the way to repeat-pass bistatic SAR interferometry, in which pairs of bistatic SAR acquisitions are used. Finally, in the last decade, both public space agencies and private leading companies are planning to launch innovative spaceborne SAR systems working in bistatic acquisition geometries, such as the X-band PLATiNO-1 (PLT-1) designed by the Italian Space Agency (ASI), that will form a bistatic SAR system with the satellites of Cosmo-SkyMed Second Generation (CSG), also working in X-band [11]. Remarkably, CSG/PLT-1 is planned to operate in two different phases: Phase 1, where PLT-1 will acquire bistatic data flying on the same orbit of CSG at a planned along-track distance of few hundreds of kilometers, and Phase 2, where PLT-1 will operate in a nominal monostatic mode on a lower orbit of about 400 km with potential bistatic modalities when sufficiently close to CSG.

In this work, we consider the general case of two closely spaced transmitters and two closely spaced receivers placed at arbitrary distance from the transmitters. This general configuration can be easily specialized to obtain all the SAR interferometry configurations described above. Indeed, the couples of transmitters and of receivers might each represent either a couple of physically separated platforms or the same platform at two different passages over the same surveyed area.

One of the main factors influencing the accuracy of interferometric measurements is coherency. The latter may be impaired by several decorrelation sources, among which baseline, or spatial, decorrelation is unavoidable, because it is caused by the fact itself that the two transmitters and/or the two receivers are spatially separated [2], [12], [13]. The analysis

Received 12 April 2024; revised 31 July 2024 and 25 September 2024; accepted 3 November 2024. Date of publication 12 November 2024; date of current version 25 November 2024. This work was supported by the Italian Space Agency (ASI) through the Project "SimulAzione e Modellazione del Sistema BistAtico COSMO-SkyMed/Platino (SAMBA)", under Grant F63C23000860001. *(Corresponding author: Alessio Di Simone.)*

The authors are with the Department of Electrical Engineering and Information Technology, University of Naples Federico II, 80125 Naples, Italy (e-mail: gerardo.dimartino@unina.it; alessio.disimone@unina.it; iodice@unina.it).

Digital Object Identifier 10.1109/TGRS.2024.3496256

© 2024 The Authors. This work is licensed under a Creative Commons Attribution-NonCommercial-NoDerivatives 4.0 License.
For more information, see https://creativecommons.org/licenses/by-nc-nd/4.0/

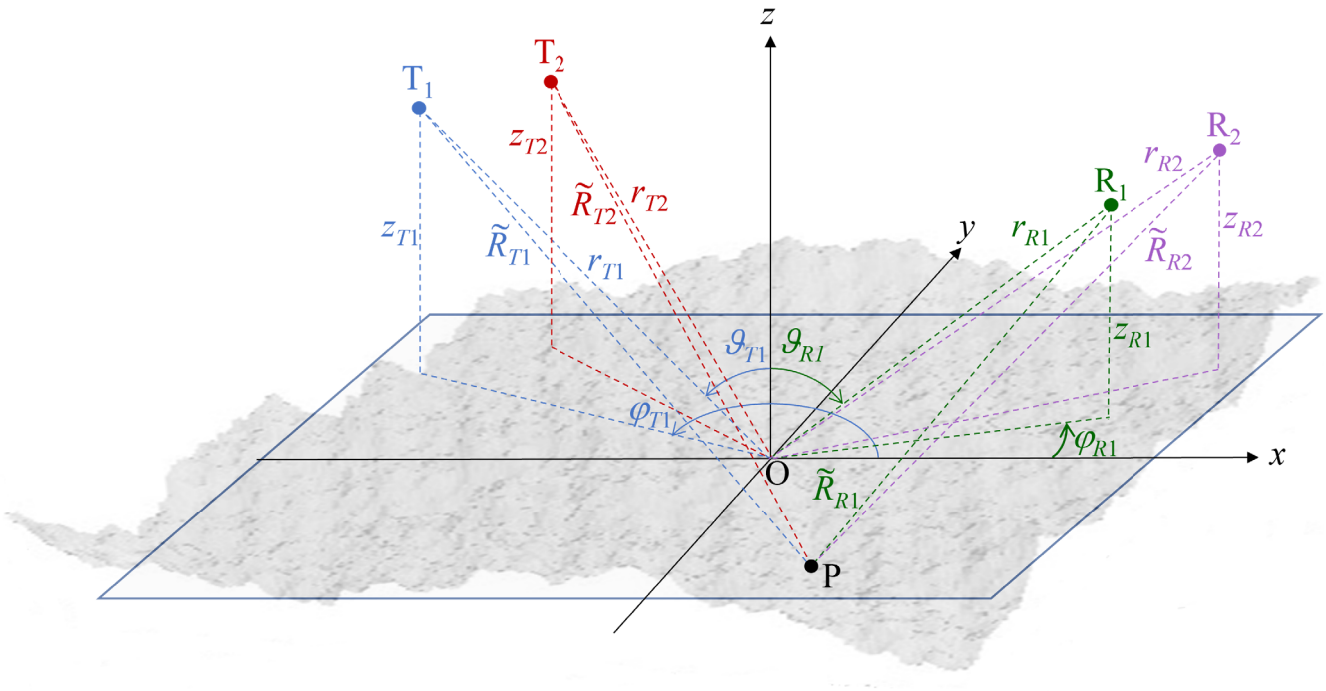

Fig. 1. Geometry of the problem.

of the correlation between the scattered fields has been the subject of intense research activities in the nineties, when different numerical, experimental, and analytical approaches for the evaluation of the so-called angular correlation function have been developed, see [14], [15], [16], [17], and [18]. Ishimaru and Chen [14] and Le et al. [17] focus on the analysis of the fields scattered in the incidence plane, while in [15] and [16] only 1-D surfaces are treated. Finally, [18] derives analytical expressions of the correlation under the small perturbation method. An evaluation of the baseline decorrelation in monostatic SAR interferometry is available in [2], [12], and [13]. In particular, in [2] and [12], it is assumed that the scattering centers belong to a flat surface and their contribution is spatially delta-correlated, whereas in [13] the scattering surface is described as randomly rough. Results of [13] reduce to those of [2] and [12] when surface standard deviation and correlation length are both much smaller than the system resolution, as it is often the case. The approach of [13] has been recently extended to the case of one transmitter and two receivers at near-specular direction [19], [20], which is the case of interest for Global Navigation Satellite System Reflectometry (GNSS-R), but not for SAR interferometry. A more general configuration is briefly considered in [21], where only the single-transmitter case is still considered. Here, we extend the approach of [13] to the general case of two transmitters and two receivers, so being able to evaluate the baseline decorrelation for both single-pass and repeat-pass bistatic SAR interferometry.

II. Theory

Let us consider a rough surface $z(x, y)$, whose mean plane is the xy plane, modeled as a statistically homogeneous zero-mean Gaussian random process with standard deviation σ and normalized (to σ^2) autocorrelation function $C(\Delta x, \Delta y)$, with $\Delta x = x' - x$, $\Delta y = y' - y$, (x, y) and (x', y') being two generic surface points. Although it is not strictly necessary, we will assume that the surface is statistically isotropic, so that $C(\Delta x, \Delta y) = C(\Delta x^2 + \Delta y^2)$. The normalized autocorrelation function is equal to one for $\Delta x = \Delta y = 0$ and is negligible for Δx and/or Δy larger than the surface correlation length L. We assume that L is much smaller than system resolution.

The geometry of the problem is depicted in Fig. 1: we consider two identical closely spaced transmitters T1 and T2, placed at $\mathbf{r}_{T1} \equiv (x_{T1}, y_{T1}, z_{T1})$, with $x_{T1} = r_{T1} \sin\vartheta_{T1} \cos\phi_{T1}$, $y_{T1} = r_{T1} \sin\vartheta_{T1} \sin\phi_{T1}$, $z_{T1} = r_{T1} \cos\vartheta_{T1}$, and $\mathbf{r}_{T2} \equiv (x_{T2}, y_{T2}, z_{T2})$, with $x_{T2} = r_{T2} \sin\vartheta_{T2} \cos\phi_{T2}$, $y_{T2} = r_{T2} \sin\vartheta_{T2} \sin\phi_{T2}$, $z_{T2} = r_{T2} \cos\vartheta_{T2}$; and two identical closely spaced receivers R1 and R2, placed at $\mathbf{r}_{R1} \equiv (x_{R1}, y_{R1}, z_{R1})$, with $x_{R1} = r_{R1} \sin\vartheta_{R1} \cos\phi_{R1}$, $y_{R1} = r_{R1} \sin\vartheta_{R1} \sin\phi_{R1}$, $z_{R1} = r_{R1} \cos\vartheta_{R1}$, and $\mathbf{r}_{R2} \equiv (x_{R2}, y_{R2}, z_{R2})$, with $x_{R2} = r_{R2} \sin\vartheta_{R2} \cos\phi_{R2}$, $y_{R2} = r_{R2} \sin\vartheta_{R2} \sin\phi_{R2}$, $z_{R2} = r_{R2} \cos\vartheta_{R2}$. We also define the transmitter baseline vector $\mathbf{B}_T = \mathbf{r}_{T2} - \mathbf{r}_{T1}$ and the receiver baseline vector $\mathbf{B}_R = \mathbf{r}_{R2} - \mathbf{r}_{R1}$, and we assume that the spacing between the transmitters is much smaller than their distances from the ground ($|\mathbf{B}_T| \ll r_{T1}, r_{T2}$), and similarly that the spacing between the receivers is much smaller than their distances from the ground ($|\mathbf{B}_R| \ll r_{R1}, r_{R2}$), so that

$$\begin{aligned} r_{T2} - r_{T1} &= B_{T\parallel} \\ \vartheta_{T2} - \vartheta_{T1} &= \Delta\vartheta_T \cong \frac{B_{T\perp}}{r_{T1}} \\ \varphi_{T2} - \varphi_{T1} &= \Delta\varphi_T \cong \frac{B_{Taz}}{r_{T1} \sin\vartheta_{T1}} \end{aligned} \tag{1}$$

and

$$\begin{aligned} r_{R2} - r_{R1} &= B_{R\parallel} \\ \vartheta_{R2} - \vartheta_{R1} &= \Delta\vartheta_R \cong \frac{B_{R\perp}}{r_{R1}} \\ \varphi_{R2} - \varphi_{R1} &= \Delta\varphi_R \cong \frac{B_{Raz}}{r_{R1}\sin\vartheta_{R1}} \end{aligned} \tag{2}$$

where $B_{T\parallel}$, $B_{T\perp}$, B_{Taz} and $B_{R\parallel}$, $B_{R\perp}$, B_{Raz} are the parallel, perpendicular, and azimuth components of the baseline vectors

$$\begin{aligned} \mathbf{B}_T &= B_{T\parallel}\hat{\mathbf{r}}_{T1} + B_{T\perp}\hat{\boldsymbol{\vartheta}}_{T1} + B_{Taz}\hat{\boldsymbol{\varphi}}_{T1} \\ \mathbf{B}_R &= B_{R\parallel}\hat{\mathbf{r}}_{R1} + B_{R\perp}\hat{\boldsymbol{\vartheta}}_{R1} + B_{Raz}\hat{\boldsymbol{\varphi}}_{R1}. \end{aligned} \tag{3}$$

The origin O of the reference system coincides with the center of the considered resolution cell. We assume perfect coregistration of the image pair, so that the center of the resolution cell is the same for both images.

By using the Kirchhoff approximation (KA) [22], the generic component of the field $E_1(\mathbf{r}_{R1})$ transmitted by T1 and scattered toward R1 can be written as

$$\begin{aligned} &E_1(\mathbf{r}_{R1}) \\ &= \int_{-\infty}^{\infty}\int_{-\infty}^{\infty} F_1(x,y) \\ &\quad \times w(x,y)\frac{\exp\{-jk[\tilde{R}_{T1}(x,y)+\tilde{R}_{R1}(x,y)]\}}{\tilde{R}_{T1}(x,y)\tilde{R}_{R1}(x,y)}dxdy. \end{aligned} \tag{4}$$

Similarly, the generic component of the field $E_2(\mathbf{r}_{R2})$ transmitted by $T2$ and scattered toward $R2$ can be written as

$$\begin{aligned} &E_2(\mathbf{r}_{R2}) \\ &= \int_{-\infty}^{\infty}\int_{-\infty}^{\infty} F_2(x,y) \\ &\quad \times w(x,y)\frac{\exp\{-jk[\tilde{R}_{T2}(x,y)+\tilde{R}_{R2}(x,y)]\}}{\tilde{R}_{T2}(x,y)\tilde{R}_{R2}(x,y)}dxdy. \end{aligned} \tag{5}$$

In (4) and (5), we have that:

1) $k = 2\pi/\lambda$ is the wavenumber, with λ being the wavelength.
2) $w(x,y)$ is the sensor illumination function, whose shape may be irregular, depending on the observation geometry and on the platforms' flight directions. In addition, even considering perfect coregistration, it may slightly differ for the two transmitter-receiver pairs. However, for not very large transmitter and receiver baselines, the assumption of equal shapes is usually acceptable. We will consider the case of arbitrary illumination function, assuming that its x and y sizes are A_x and A_y, respectively, but we will also specialize the obtained expressions in the Gaussian case

$$w(x,y) = \exp\left(-\frac{x^2}{2A_x^2} - \frac{y^2}{2A_y^2}\right). \tag{6}$$

3)

$$\begin{aligned} \tilde{R}_X(x,y) &= \sqrt{(z_X - z)^2 + (x_X - x)^2 + (y_X - y)^2} \\ &= R_X(x,y)\sqrt{1 + \frac{z^2 - 2z_X z}{R_X^2(x,y)}} \cong \\ &\cong R_X(x,y) - \frac{z_X}{R_X(x,y)}z(x,y) \end{aligned} \tag{7}$$

with

$$R_X(x,y) = \sqrt{z_X^2 + (x_X - x)^2 + (y_X - y)^2} \tag{8}$$

and with the subscript X that must be replaced by $T1$, $T2$, $R1$, or $R2$ as needed, so that r_X are the distances of sensors from the origin, R_X are their distances from the generic point $(x, y, 0)$ of the mean plane, and $\tilde{R}_X$ are their distances from the generic point $[x, y, z(x,y)]$ of the rough surface;

4) $F_{1,2}(x,y)$ are slowly varying functions, proportional to the incident field, accounting for the polarizations of both the incident and scattered field, the look angles $\vartheta_{T1,2}$, the receivers polar $\vartheta_{R1,2}$ and azimuth angles $\varphi_{R1,2}$, the local slopes of the surface and its dielectric properties through the local Fresnel reflection coefficients. However, its expressions, as shown in the following, are of no interest for our purposes. The interested reader can find more details in [22].

We explicitly note that the same formulation, (4) and (5), can be obtained under the first-order small-slope approximation (SSA1) [23], with different expressions of the slowly varying function $F_{1,2}(x,y)$. This ensures that our results for the correlation coefficient are valid under both the KA and the SSA1.

It is also important to note that the functions $F_{1,2}(x,y)$ and $R_X(x,y)$ are slowly spatially varying, that is, they appreciably change only for variations of x and y not much smaller than the $R1$ distance r_{R1}. Accordingly, the variations of such functions over distances much smaller than r_{R1} can be ignored, except that in the argument of the complex exponential functions in (4) and (5), where variations of $R_X(x,y)$ can be only ignored if they are much smaller than wavelength.

We want now to compute the correlation coefficient

$$\rho = \frac{|\mathrm{cov}[E_1(\mathbf{r}_{R1}), E_2(\mathbf{r}_{R2})]|}{\sqrt{\mathrm{var}[E_1(\mathbf{r}_{R1})]\mathrm{var}[E_2(\mathbf{r}_{R2})]}} \tag{9}$$

where

$$\begin{aligned} &\mathrm{cov}[E_1(\mathbf{r}_{R1}), E_2(\mathbf{r}_{R2})] \\ &= \left\langle [E_1(\mathbf{r}_{R1}) - \langle E_1(\mathbf{r}_{R1})\rangle][E_2(\mathbf{r}_{R2}) - \langle E_2(\mathbf{r}_{R2})\rangle]^*\right\rangle \\ &= \left\langle E_1(\mathbf{r}_{R1})E_2(\mathbf{r}_{R2})^*\right\rangle - \langle E_1(\mathbf{r}_{R1})\rangle\langle E_2(\mathbf{r}_{R2})\rangle^* \end{aligned} \tag{10}$$

$$\begin{aligned} \mathrm{var}\left[E_{1,2}(\mathbf{r}_{R1,2})\right] &= \left\langle \left|E_{1,2}(\mathbf{r}_{R1,2}) - \left\langle E_{1,2}(\mathbf{r}_{R1,2})\right\rangle\right|^2\right\rangle \\ &= \left\langle \left|E_{1,2}(\mathbf{r}_{R1,2})\right|^2\right\rangle - \left|\left\langle E_{1,2}(\mathbf{r}_{R1,2})\right\rangle\right|^2 \end{aligned} \tag{11}$$

and the symbol $\langle\cdot\rangle$ indicates the statistical mean (i.e., the ensemble average).

By using (4) and (5) in (10), we get

$$\begin{aligned} &\mathrm{cov}[E_1(\mathbf{r}_{R1}), E_2(\mathbf{r}_{R2})] \cong \int_{-\infty}^{\infty}\int_{-\infty}^{\infty}\int_{-\infty}^{\infty}\int_{-\infty}^{\infty} \\ &\frac{\exp\{-jk[R_{T1}(x,y)+R_{R1}(x,y)-R_{T2}(x',y')-R_{R2}(x',y')]\}}{R_{T1}(x,y)R_{T2}(x'y')R_{R1}(x,y)R_{R2}(x',y')} \end{aligned}$$

$$\times F_1(x,y)w(x,y)F_2^*(x',y')w(x',y')$$
$$\times\left[\left\langle\exp\left\{jk\left[u_{z1}(x,y)z(x,y)-u_{z2}(x',y')z(x',y')\right]\right\}\right\rangle$$
$$-\left\langle\exp\left\{jk\left[u_{z1}(x,y)z(x,y)\right]\right\}\right\rangle$$
$$\times\left\langle\exp\left\{-jk\left[u_{z2}(x',y')z(x',y')\right]\right\}\right\rangle\Big]dxdydx'dy' \quad (12)$$

where

$$u_{z1,2}(x,y)=\frac{z_{T1,2}}{R_{T1,2}(x,y)}+\frac{z_{R1,2}}{R_{R1,2}(x,y)}. \quad (13)$$

It should be noted that each term in $u_{z1,2}$ in (13) comes from the approximation of the sensor-surface point distance $\tilde{R}$ in (7). Indeed, they allow to express the sensor-surface point distance $\tilde{R}$ in terms of the distance R between the sensor and the mean plane point corresponding to the generic surface point. Consequently, $u_{z1,2}$ allows to write the actual bistatic range in terms of the bistatic range evaluated over the mean plane.

Let us now focus on the following function that appears in (12):

$$f(x,y,x',y')$$
$$=\left\langle\exp\left\{jk\left[u_{z1}(x,y)z(x,y)-u_{z2}(x',y')z(x',y')\right]\right\}\right\rangle$$
$$-\left\langle\exp\left\{jk\left[u_{z1}(x,y)z(x,y)\right]\right\}\right\rangle$$
$$\times\left\langle\exp\left\{-jk\left[u_{z2}(x',y')z(x',y')\right]\right\}\right\rangle.$$

The statistical means that appear in this expression are the characteristic functions [24] of Gaussian random variables, so that they can be readily computed

$$f(x,y,x',y')$$
$$=\exp\left\{-\frac{k^2\sigma^2}{2}\left[u_{z1}^2(x,y)+u_{z2}^2(x',y')\right.\right.$$
$$\left.\left.-2u_{z1}(x,y)u_{z2}(x',y')C(\Delta x,\Delta y)\right]\right\}$$
$$-\exp\left\{-\frac{k^2\sigma^2}{2}\left[u_{z1}^2(x,y)+u_{z2}^2(x',y')\right]\right\}$$
$$=\exp\left\{-\frac{k^2\sigma^2}{2}\left[u_{z1}(x,y)-u_{z2}(x',y')\right]^2\right\}$$
$$\times\left[\exp\left\{-k^2\sigma^2u_{z1}(x,y)u_{z2}(x',y')\left[1-C(\Delta x,\Delta y)\right]\right\}\right.$$
$$\left.-\exp\left\{-k^2\sigma^2u_{z1}(x,y)u_{z2}(x',y')\right\}\right]. \quad (14)$$

The function f is appreciably different from zero only for Δx and Δy not larger than the surface correlation length L, where $C(\Delta x,\Delta y)$ is not negligible. Therefore, the integrand of (12) is appreciably different from zero only for $|x-x'|$ and $|y-y'|$ smaller than L. Considering that L is much smaller than resolution, which in turns is usually much smaller than the transmitter and receiver distances r_{T1} and r_{R1}, in the first exponential of (12), we can let

$$R_{T1}(x,y)+R_{R1}(x,y)-R_{T2}(x',y')-R_{R2}(x',y')$$
$$=R_{T1}(x,y)+R_{R1}(x,y)-R_{T1}(x',y')-R_{R1}(x',y')$$
$$+R_{T1}(x',y')-R_{T2}(x',y')+R_{R1}(x',y')-R_{R2}(x',y')$$
$$\cong -u_x(x,y)\Delta x-u_y(x,y)\Delta y+R_{T1}(x,y)-R_{T2}(x,y)$$
$$+R_{R1}(x,y)-R_{R2}(x,y) \quad (15)$$

where

$$u_x(x,y)=\frac{\partial(R_{T1}+R_{R1})}{\partial x}=\frac{x-x_{T1}}{R_{T1}(x,y)}+\frac{x-x_{R1}}{R_{R1}(x,y)}$$

$$u_y(x,y)=\frac{\partial(R_{T1}+R_{R1})}{\partial y}=\frac{y-y_{T1}}{R_{T1}(x,y)}+\frac{y-y_{R1}}{R_{R1}(x,y)}. \quad (16)$$

In addition, elsewhere in (12) and (14), apart from $C(\Delta x,\Delta y)$, we can assume $x=x'$, $y=y'$. It is worth stressing here that similar approaches allowing to reduce the fourfold integral in (12) to a twofold one have been proposed in the literature, see [12], [13], and [18]. Accordingly, (14) can be rewritten as

$$f(x,y,x',y')$$
$$=\exp\left\{-\frac{k^2\sigma^2}{2}\left[u_{z1}(x,y)-u_{z2}(x,y)\right]^2\right\}\tilde{f}(x,y,\Delta x,\Delta y) \quad (17)$$

where

$$\tilde{f}(x,y,\Delta x,\Delta y)$$
$$=\left[\exp\left\{-k^2\sigma^2u_z^2(x,y)\left[1-C(\Delta x,\Delta y)\right]\right\}\right.$$
$$\left.-\exp\left\{-k^2\sigma^2u_z^2(x,y)\right\}\right] \quad (18)$$

and we have set $u_z(x,y)=(u_{z1}(x,y)u_{z2}(x,y))^{1/2}$.

Note that in (15), we have set $R_{T1}(x',y')-R_{T2}(x',y')\cong R_{T1}(x,y)-R_{T2}(x,y)$ and $R_{R1}(x',y')-R_{R2}(x',y')\cong R_{R1}(x,y)-R_{R2}(x,y)$. It can be shown that the corresponding errors are of the order of $(|\mathbf{B}_T|/r_{T1})$ and $(|\mathbf{B}_R|/r_{R1})$ times the distance from (x,y) to (x',y'), respectively. Therefore, our approximation holds if $(|\mathbf{B}_T|/r_{T1})L$ and $(|\mathbf{B}_R|/r_{R1})L$ do not exceed λ. For example, for systems with baselines of the order of some kilometers, L cannot exceed a few meters.

By using (15) and (17) in (12), we have

$$\mathrm{cov}[E_1(\mathbf{r}_{R1}),E_2(\mathbf{r}_{R2})]$$
$$\cong\int_{-\infty}^{\infty}\int_{-\infty}^{\infty}\frac{F_1(x,y)F_2^*(x,y)w^2(x,y)}{R_{T1}(x,y)R_{T2}(x,y)R_{R1}(x,y)R_{R2}(x,y)}$$
$$\times\exp\left\{-jk\left[R_{T1}(x,y)-R_{T2}(x,y)+R_{R1}(x,y)-R_{R2}(x,y)\right]\right\}$$
$$\times\exp\left\{-\frac{k^2\sigma^2}{2}\left[u_{z1}(x,y)-u_{z2}(x,y)\right]^2\right\}$$
$$\times\int_{-\infty}^{\infty}\int_{-\infty}^{\infty}\exp\left[jku_x(x,y)\Delta x\right]\exp\left[jku_y(x,y)\Delta y\right]$$
$$\times\tilde{f}(x,y,\Delta x,\Delta y)d\Delta xd\Delta ydxdy. \quad (19)$$

The double integral over Δx and Δy in (19) is the Fourier transform (FT) of $\tilde{f}(x,y,\Delta x,\Delta y)$ evaluated in $ku_x(x,y)$, $ku_y(x,y)$, so that we can write

$$\mathrm{cov}[E_1(\mathbf{r}_{R1}),E_2(\mathbf{r}_{R2})]$$
$$\cong\int_{-\infty}^{\infty}\int_{-\infty}^{\infty}\frac{F_1(x,y)F_2^*(x,y)w^2(x,y)}{R_{T1}(x,y)R_{T2}(x,y)R_{R1}(x,y)R_{R2}(x,y)}$$
$$\times\exp\left\{-jk\left[R_{T1}(x,y)-R_{T2}(x,y)\right.\right.$$
$$\left.\left.+R_{R1}(x,y)-R_{R2}(x,y)\right]\right\}$$
$$\times\exp\left\{-\frac{k^2\sigma^2}{2}\left[u_{z1}(x,y)-u_{z2}(x,y)\right]^2\right\}$$
$$\times\tilde{F}\left(x,y,ku_x(x,y),ku_y(x,y)\right)dxdy \quad (20)$$

where $\tilde{F}$ is the FT of $\tilde{f}$ (and it is real, due to the symmetry properties of the autocorrelation function). The sensor illumination function w in (20) is peaked around the origin and is appreciably different from zero only in the resolution cell of

area of the order of $A_x A_y$. Since the resolution is usually much smaller than r_{T1} and r_{R1}, in the resolution cell the argument of the first exponential in (20) can be approximated by expanding it around the origin

$$\begin{aligned} &R_{T1}(x,y) - R_{T2}(x,y) + R_{R1}(x,y) - R_{R2}(x,y) \\ &\quad \cong r_{T1} - r_{T2} + r_{R1} - r_{R2} + \eta_x x + \eta_y y \end{aligned} \tag{21}$$

where $\eta_x = \eta_{Tx} + \eta_{Rx}$ and $\eta_y = \eta_{Ty} + \eta_{Ry}$ with

$$\begin{aligned} \eta_{Tx} &= \left.\frac{\partial(R_{T1} - R_{T2})}{\partial x}\right|_{\substack{x=0\\y=0}} = -\frac{x_{T1}}{r_{T1}} + \frac{x_{T2}}{r_{T2}} \\ &= -\sin\vartheta_{T1}\cos\varphi_{T1} + \sin\vartheta_{T2}\cos\varphi_{T2} \\ &\cong \cos\vartheta_{T1}\cos\varphi_{T1}\Delta\vartheta_T - \sin\vartheta_{T1}\sin\varphi_{T1}\Delta\varphi_T \cong \\ &\cong \frac{\cos\vartheta_{T1}\cos\varphi_{T1}B_{T\perp}}{r_{T1}} - \frac{\sin\varphi_{T1}B_{Taz}}{r_{T1}} \\ \eta_{Ty} &= \left.\frac{\partial(R_{T1} - R_{T2})}{\partial y}\right|_{\substack{x=0\\y=0}} \\ &= -\frac{y_{T1}}{r_{T1}} + \frac{y_{T2}}{r_{T2}} = -\sin\vartheta_{T1}\sin\varphi_{T1} + \sin\vartheta_{T2}\sin\varphi_{T2} \\ &\cong \cos\vartheta_{T1}\sin\varphi_{T1}\Delta\vartheta_T + \sin\vartheta_{T1}\cos\varphi_{T1}\Delta\varphi_T \\ &\cong \frac{\cos\vartheta_{T1}\sin\varphi_{T1}B_{T\perp}}{r_{T1}} + \frac{\cos\varphi_{T1}B_{Taz}}{r_{T1}} \end{aligned} \tag{22}$$

η_{Rx} and η_{Ry} being obtained from (22) by replacing the subscript $T1$ and $T2$ with $R1$ and $R2$, respectively.

The parameters η_x and η_y allow to simplify the distances R_X in (21) by expressing them in terms of the sensor-origin distances r_X.

All other functions in (20) can be assumed approximately constant in the resolution cell and equal to their value in the origin

$$F_{1,2}(x,y) \cong F_{1,2}(0,0) = F_{10,20} \tag{23}$$

$$\begin{aligned} &u_{z1}(x,y) - u_{z2}(x,y) \\ &\quad \cong u_{z1}(0,0) - u_{z2}(0,0) \\ &\quad = \cos\vartheta_{T1} + \cos\vartheta_{R1} - \cos\vartheta_{T2} - \cos\vartheta_{R2} \\ &\quad \cong \sin\vartheta_{T1}\Delta\vartheta_T + \sin\vartheta_{R1}\Delta\vartheta_R \\ &\quad \cong \frac{\sin\vartheta_{T1}B_{T\perp}}{r_{T1}} + \frac{\sin\vartheta_{R1}B_{R\perp}}{r_{R1}} \end{aligned} \tag{24}$$

$$\begin{aligned} &u_z(x,y) \\ &\quad \cong u_{z0} = u_z(0,0) \cong \cos\vartheta_{T1} + \cos\vartheta_{R1} \end{aligned} \tag{25}$$

$$\begin{aligned} &u_x(x,y) \\ &\quad \cong u_{x0} = u_x(0,0) \\ &\quad = -\sin\vartheta_{T1}\cos\varphi_{T1} - \sin\vartheta_{R1}\cos\varphi_{R1} \end{aligned} \tag{26}$$

$$\begin{aligned} &u_y(x,y) \cong u_{y0} = u_y(0,0) \\ &\quad = -\sin\vartheta_{T1}\sin\varphi_{T1} - \sin\vartheta_{R1}\sin\varphi_{R1} \end{aligned} \tag{27}$$

$$\begin{aligned} &\tilde{F}\big(x,y,ku_x(x,y),ku_y(x,y)\big) \cong \tilde{F}_0 \\ &\quad = \tilde{F}\big(0,0,ku_{x0},ku_{y0}\big). \end{aligned} \tag{28}$$

By using (21), (23)–(28) in (20) we get

$$\begin{aligned} &\operatorname{cov}[E_1(\mathbf{r}_{R1}), E_2(\mathbf{r}_{R2})] \\ &\cong \frac{F_{10}F_{20}^*\tilde{F}_0\exp\left[-jk(r_{T1} - r_{T2} + r_{R1} - r_{R2})\right]}{r_{T1}r_{T2}r_{R1}r_{R2}} \\ &\quad \times \exp\left\{-\frac{k^2\sigma^2}{2}\left[\frac{\sin\vartheta_{T1}B_{T\perp}}{r_{T1}} + \frac{\sin\vartheta_{R1}B_{R\perp}}{r_{R1}}\right]^2\right\} \\ &\quad \times \int_{-\infty}^{\infty}\int_{-\infty}^{\infty} w^2(x,y)\exp\left[-jk\eta_x x - jk\eta_y y\right]dxdy. \end{aligned} \tag{29}$$

The double integral over x and y in (29) is the FT of $w^2(x,y)$ evaluated in $k\eta_x$, $k\eta_y$, so that we can write, by using also (22)

$$\begin{aligned} &\operatorname{cov}[E_1(\mathbf{r}_{R1}), E_2(\mathbf{r}_{R2})] \\ &= \frac{F_{10}F_{20}^*\tilde{F}_0\exp\left[jk\left(B_{T\parallel} + B_{R\parallel}\right)\right]}{r_{T1}r_{T2}r_{R1}r_{R2}} \\ &\quad \times \exp\left\{-\frac{k^2\sigma^2}{2}\left[\frac{\sin\vartheta_{T1}B_{T\perp}}{r_{T1}} + \frac{\sin\vartheta_{R1}B_{R\perp}}{r_{R1}}\right]^2\right\} \\ &\quad \times W_{\mathrm{sq}}\left\{k\left[\frac{\cos\vartheta_{T1}\cos\varphi_{T1}B_{T\perp}}{r_{T1}} - \frac{\sin\varphi_{T1}B_{Taz}}{r_{T1}}\right.\right. \\ &\qquad \left. + \frac{\cos\vartheta_{R1}\cos\varphi_{R1}B_{R\perp}}{r_{R1}} - \frac{\sin\varphi_{R1}B_{Raz}}{r_{R1}}\right], \\ &\qquad k\left[\frac{\cos\vartheta_{T1}\sin\varphi_{T1}B_{T\perp}}{r_{T1}} + \frac{\cos\varphi_{T1}B_{Taz}}{r_{T1}}\right. \\ &\qquad \left.\left. + \frac{\cos\vartheta_{R1}\sin\varphi_{R1}B_{R\perp}}{r_{R1}} + \frac{\cos\varphi_{R1}B_{Raz}}{r_{R1}}\right]\right\} \end{aligned} \tag{30}$$

where $\mathrm{W}_{\mathrm{sq}}(k\eta_x, k\eta_y)$ is the FT of the sensor illumination function squared $w^2(x,y)$.

The field variances are easily deduced from (30) by setting all baselines to zero

$$\operatorname{var}\left[E_{1,2}\left(\mathbf{r}_{R1,R2}\right)\right] \cong \frac{\left|F_{10,20}\right|^2\left|\mathrm{W}_{\mathrm{sq}}(0,0)\right|\tilde{F}_0}{r_{T1,T2}^2 r_{R1,R2}^2}. \tag{31}$$

By replacing (30) and (31) in (9), we finally get

$$\begin{aligned} \rho &\cong \exp\left\{-\frac{k^2\sigma^2}{2}\left[\frac{\sin\vartheta_{T1}B_{T\perp}}{r_{T1}} + \frac{\sin\vartheta_{R1}B_{R\perp}}{r_{R1}}\right]^2\right\} \\ &\quad \times \left|\mathrm{W}_{\mathrm{sq}}\left\{k\left[\frac{\cos\vartheta_{T1}\cos\varphi_{T1}B_{T\perp}}{r_{T1}} - \frac{\sin\varphi_{T1}B_{Taz}}{r_{T1}}\right.\right.\right. \\ &\qquad \left. + \frac{\cos\vartheta_{R1}\cos\varphi_{R1}B_{R\perp}}{r_{R1}} - \frac{\sin\varphi_{R1}B_{Raz}}{r_{R1}}\right], \\ &\qquad k\left[\frac{\cos\vartheta_{T1}\sin\varphi_{T1}B_{T\perp}}{r_{T1}} + \frac{\cos\varphi_{T1}B_{Taz}}{r_{T1}} + \frac{\cos\vartheta_{R1}\sin\varphi_{R1}B_{R\perp}}{r_{R1}}\right. \\ &\qquad \left.\left.\left. + \frac{\cos\varphi_{R1}B_{Raz}}{r_{R1}}\right]\right\}/\mathrm{W}_{\mathrm{sq}}(0,0)\right|. \end{aligned} \tag{32}$$

By using a well-known property of the FT, that is, the uncertainty principle, we can state that $\mathrm{W}_{\mathrm{sq}}(k\eta_x, k\eta_y)$ is appreciably different from zero only if $k\eta_x$ is not larger than a critical value of the order of $1/A_x$ and if, at the same time, $k\eta_y$ is not larger than a critical value of the order of $1/A_y$. For instance, if the Gaussian illumination function of (6) is considered, we get

$$\mathrm{W}_{\mathrm{sq}}\left(k\eta_x, k\eta_y\right) = \pi A_x A_y \exp\left\{-\frac{k^2\eta_x^2 A_x^2}{4} - \frac{k^2\eta_y^2 A_y^2}{4}\right\} \tag{33}$$

and the critical values for $k\eta_x$ and $k\eta_y$ are $2/A_x$ and $2/A_y$, respectively.

With simple algebraic manipulations, it can be shown that, if $A_x = A_y$ and $B_{Taz} = B_{Raz} = 0$, the correlation coefficient in (32) and (33) does not depend on the $T1$ and $R1$ azimuth angle separately, but only on their difference $\varphi_{T1} - \varphi_{R1}$. If, additionally, $B_{T\perp} = 0$, that is, in the presence of one transmitter, the correlation coefficient is independent of the R1 azimuth angle φ_{R1}.

Equations (32) and (33) allow computing the correlation coefficient for a very general bistatic geometry, but they are quite involved due to the involved expressions in (22). However, they can be greatly simplified if we make some reasonable assumptions. First of all, with no significant loss of generality, we can assume that the $T1$ azimuth angle $\varphi_{T1} = 0$. In addition, in most cases, it is reasonable to assume that the surface standard deviation is much smaller than the system resolution along x, that is, $\sigma \ll A_x$, so that (apart from a particular case that we will consider later) the first exponential in (32) can be assumed unitary when the second one is nonnegligible. Finally, we assume that azimuth baselines are null, that is, $B_{Taz} = B_{Raz} = 0$. With these assumptions, (32) simplifies as

$$\rho \cong \left| \mathrm{W_{sq}} \left\{ k \left[\frac{\cos\vartheta_{T1} B_{T\perp}}{r_{T1}} + \frac{\cos\vartheta_{R1}\cos\varphi_{R1} B_{R\perp}}{r_{R1}} \right], k \left[\frac{\cos\vartheta_{R1}\sin\varphi_{R1} B_{R\perp}}{r_{R1}} \right] \right\} / \mathrm{W_{sq}}(0,0) \right| = \\ = \exp\left\{ -\frac{k^2 A_x^2}{4} \left[\frac{\cos\vartheta_{T1} B_{T\perp}}{r_{T1}} + \frac{\cos\vartheta_{R1}\cos\varphi_{R1} B_{R\perp}}{r_{R1}} \right]^2 - \frac{k^2 A_y^2}{4} \left[\frac{\cos\vartheta_{R1}\sin\varphi_{R1} B_{R\perp}}{r_{R1}} \right]^2 \right\} \tag{34}$$

where the second equality holds for the Gaussian illumination function of (6).

III. Discussion

Before going further in the discussion of the derived formulation, it is helpful to summarize the main mathematical steps leading to (34).

First of all, we have focused on the evaluation of the correlation coefficient over such natural scenes where single surface scattering is the dominant contribution, such as bare soil surfaces or scarcely to moderately vegetated areas; additionally, we treated the most general bistatic SAR system comprising two transmitters and two receivers.

In order to keep the mathematical treatability of the problem, we made the following assumptions.

1) *H.1:* KA or SSA-1 holds.
2) *H.2:* The resolution cell sizes along x and y, A_x, A_y are much smaller than r_{T1}, r_{R1}.
3) *H.3:* The surface correlation length L is much smaller than system resolution.
4) *H.4:* $|\mathbf{B}_\mathrm{T}| \ll r_{T1}$ and $|\mathbf{B}_\mathrm{R}| \ll r_{R1}$, where the system baselines are defined in (3).

By means of KA (or SSA-1), the field received by the two receivers can be written as in (4) and (5) and their correlation coefficient can be evaluated through (9) by definition, where the covariance is reported in (12) and the variances can be obtained by setting all the baselines to zero.

Exploiting the hypotheses H.2–H.4, the covariance can be simplified as in (29), that immediately leads to (30) by introducing the FT of the illumination function squared. By replacing (30) and (31) in (9), we obtain the final expression in (32), that specializes as in (34) in the case of Gaussian illumination, that is, (33), and if the following additional simplifying assumptions on the imaging geometry and the sensed scene hold.

1) $\varphi_{T1} = 0$.
2) $B_{Taz} = B_{Raz} = 0$.
3) $\sigma \ll A_x$.

Inspection of the final formulations in (32) and (34) reveals that the obtained correlation coefficient is independent upon the dielectric properties of the sensed surface, that is, its soil wetness. This follows from the slow variations of the $F_{1,2}(x, y)$ function, that, then, simplifies in the evaluation of the correlation coefficient, see (9), (30), and (31). Therefore, varying soil wetness will not lead to any variation of the correlation coefficient.

Similarly, if, additionally, $\sigma \ll A_x$, the correlation coefficient is independent upon the surface roughness, as well, see (34).

It is worth mentioning that surface roughness σ is on the orders from mm to cm for most natural surfaces, whereas the system resolution typically ranges from meters to tens of meters for most SAR systems. Accordingly, in most scenarios of interest here, the assumption $\sigma \ll A_x$ can be safely assumed valid. Notwithstanding, it should be noted that this simplifying hypothesis is not strictly required in our formulation as the more general formulation in (32) might be applied in the case it is not valid or if more accurate evaluations are desired. In such cases, additional information about the surface roughness is required.

In the quite general case of (34), it is not possible to define critical baselines: in order to obtain a nonnegligible coherence, we have to set

$$\begin{cases} \dfrac{\cos\vartheta_{T1} B_{T\perp}}{r_{T1}} + \dfrac{\cos\vartheta_{R1}\cos\varphi_{R1} B_{R\perp}}{r_{R1}} < \dfrac{\lambda}{\pi A_x} \\ \dfrac{\cos\vartheta_{R1}\sin\varphi_{R1} B_{R\perp}}{r_{R1}} < \dfrac{\lambda}{\pi A_y}. \end{cases} \tag{35}$$

In addition, for $\sin\varphi_{R1} \neq 0$, that is, for noncoplanar geometries, the only way to obtain a unitary correlation coefficient is having null orthogonal baselines, in which case the phase sensitivity to topography is obviously null.

Let us now consider some particular cases that are often met in existing, planned, or proposed bistatic interferometric SAR systems, such as SESAME and CSG/PLT-1.

A. Single-Pass SAR Interferometry

In single-pass monostatic or bistatic SAR interferometry, a single transmitter is present. This is also the case of some proposed systems in which two ground-based receivers collect the signal transmitted by a spaceborne SAR and scattered by

the ground [9]. In this case $B_{T\perp}=0$ and (34) becomes

$$\rho \cong \left| \frac{W_{\rm sq}\left\{ \frac{k\cos\vartheta_{R1}\cos\varphi_{R1}B_{R\perp}}{r_{R1}}, \frac{k\cos\vartheta_{R1}\sin\varphi_{R1}B_{R\perp}}{r_{R1}} \right\}}{\mathrm{W}_{\rm sq}(0,0)} \right| = \exp\left\{ -(A_x^2\cos^2\varphi_{R1}+A_y^2\sin^2\varphi_{R1}) \left[\frac{k\cos\vartheta_{R1}B_{R\perp}}{2r_{R1}} \right]^2 \right\}. \tag{36}$$

In this case, the critical baseline $B_{R\perp c}$ can be defined by equating the argument of the exponential in (36) to minus one

$$B_{R\perp c} = \frac{\lambda r_{R1}}{\pi\cos\vartheta_{R1}\sqrt{A_x^2\cos^2\varphi_{R1}+A_y^2\sin^2\varphi_{R1}}}. \tag{37}$$

The monostatic single-pass case is obtained by further letting $\varphi_{R1}=0$, $r_{R1}=r_{T1}=r_1$, and $\vartheta_{R1}=\vartheta_{T1}=\vartheta_1$, so that (36) and (37) become

$$\rho \cong \frac{W_{\rm sq}\left\{ \frac{k\cos\vartheta_1 B_{R\perp}}{r_1}, 0 \right\}}{\mathrm{W}_{\rm sq}(0,0)} = \exp\left\{ -\left[\frac{kA_x\cos\vartheta_1 B_{R\perp}}{2r_1} \right]^2 \right\} = \exp\left\{ -\left[\frac{\pi A_r B_{R\perp}}{\lambda r_1\tan\vartheta_1} \right]^2 \right\} \tag{38}$$

$$B_{R\perp c} = \frac{\lambda r_1}{\pi\cos\vartheta_1 A_x} = \frac{\lambda r_1\tan\vartheta_1}{\pi A_r} \tag{39}$$

where $A_r = c/(2\Delta f) = A_x\sin\vartheta_1$ is the slant-range resolution, with c being the speed of light and Δf the transmitted chirp bandwidth. Equation (39) is in agreement with the classical result of [2], [12], and [13] for the single-pass case (the presence of π at the denominator of (39) is due to the fact that we are considering a Gaussian, rather than sinc-type, illumination function).

B. Coplanar Geometry

Let us consider the case in which transmitters and receivers all belong to the xz plane, that is, $\varphi_{R1}=0$ (backward scattering geometry) or $\varphi_{R1}=\pi$ (forward scattering geometry), see Fig. 2. This is the case, for instance, of parallel sensors' trajectories with nonsquinted looking geometry. Remarkably, the backward geometry is relevant for the CSG/PLT-1 system when operating in repeat-pass mode in Phase 2. In this case, (34) specializes as

$$\rho \cong \frac{W_{\rm sq}\left\{ k\left[\frac{\cos\vartheta_{T1}B_{T\perp}}{r_{T1}} \pm \frac{\cos\vartheta_{R1}B_{R\perp}}{r_{R1}} \right], 0 \right\}}{\mathrm{W}_{\rm sq}(0,0)} = \exp\left\{ -\frac{k^2A_x^2}{4}\left[\frac{\cos\vartheta_{T1}B_{T\perp}}{r_{T1}} \pm \frac{\cos\vartheta_{R1}B_{R\perp}}{r_{R1}} \right]^2 \right\} \tag{40}$$

where the plus and minus signums hold for backward and forward scattering geometries, respectively. In this case, it is not possible to define critical baselines: in order to obtain a nonnegligible coherence, we have to set

$$\frac{\cos\vartheta_{T1}B_{T\perp}}{r_{T1}} \pm \frac{\cos\vartheta_{R1}B_{R\perp}}{r_{R1}} < \frac{\lambda}{\pi A_x}. \tag{41}$$

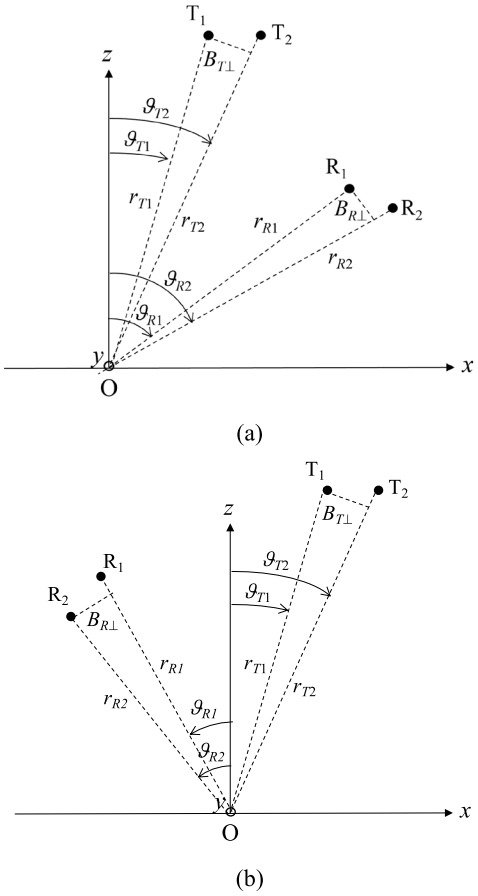

Fig. 2. Coplanar geometry (a) backward and (b) forward scattering.

In this case, the ground range resolution A_x can be related to the slant range one $A_r = c/(2\Delta f)$ as follows:

$$A_r = \frac{1}{2}|u_{x0}|A_x = \frac{|\sin\vartheta_{T1}\pm\sin\vartheta_{R1}|}{2}A_x \tag{42}$$

so that in the monostatic repeat-pass case ($\vartheta_{R1}=\vartheta_{T1}=\vartheta_1$, $r_{R1}=r_{T1}=r_1$, $B_{T\perp}=B_{R\perp}=B_\perp$ and $\varphi_{R1}=0$) we have $A_r = A_x\sin\vartheta_1$ and (40) and (41) lead to the classical result of [2], [12], and [13]

$$\rho \cong \frac{W_{\rm sq}\left\{ \frac{2k\cos\vartheta_1 B_\perp}{r_1}, 0 \right\}}{\mathrm{W}_{\rm sq}(0,0)} = \exp\left\{ -\left[\frac{kA_x\cos\vartheta_1 B_\perp}{r_1} \right]^2 \right\} = \exp\left\{ -\left[\frac{2\pi A_r B_{R\perp}}{\lambda r_1\tan\vartheta_1} \right]^2 \right\} \tag{43}$$

$$B_{R\perp c} = \frac{\lambda r_1}{2\pi\cos\vartheta_1 A_x} = \frac{\lambda r_1\tan\vartheta_1}{2\pi A_r}. \tag{44}$$

Note that in the specular case ($\vartheta_{R1}=\vartheta_{T1}=\vartheta_1$ and $\varphi_{R1}=\pi$) according to (42) the ground range resolution tends to infinity for fixed chirp bandwidth. Actually, in this case (42) is not a good approximation, but anyway ground range resolution is very bad. Therefore, this case is not considered for SAR interferometry applications, and we will ignore it here. However, the specular geometry is very useful for GNSS-R, and it is considered in detail in [19] and [20].

Quite interestingly, in the coplanar geometry, it is possible to obtain a unitary correlation coefficient with nonnull orthogonal baselines. In fact, it is sufficient that

$$\frac{\cos\vartheta_{T1}B_{T\perp}}{r_{T1}} = \mp\frac{\cos\vartheta_{R1}B_{R\perp}}{r_{R1}}. \tag{45}$$

It is worth noting that (45) unveils the relationship between the receiver and transmitter orthogonal baselines to achieve the maximum correlation coefficient. Actually, even if condition (45) is satisfied, the correlation coefficient is not exactly unitary, because of the first exponential of (32). In addition, as shown in the following, if (45) is satisfied, the phase sensitivity to topography is null.

The interferometric phase is

$$\Phi = \frac{2\pi}{\lambda}(R_{T1} + R_{R1} - R_{T2} - R_{R2}) \tag{46}$$

so that its sensitivity to topography is its rate of variation with respect to z along an equi-range line, see Fig. 3

$$\begin{aligned}\frac{\partial\Phi}{\partial z} &= \frac{2\pi}{\lambda}\frac{\partial(R_{T1} + R_{R1} - R_{T2} - R_{R2})}{\partial z} \\ &= \frac{2\pi}{\lambda}\frac{\partial(R_{T1} + R_{R1} - R_{T2} - R_{R2})}{\partial\bar{\vartheta}}\frac{\partial\bar{\vartheta}}{\partial z}\end{aligned} \tag{47}$$

where all the derivatives are computed in the origin and, see Fig. 3

$$\begin{aligned}\bar{\vartheta} &= \arctan\left(\frac{u_{x0}}{-u_{z0}}\right) = \arctan\left(\frac{\sin\vartheta_{T1} \pm \sin\vartheta_{R1}}{\cos\vartheta_{T1} + \cos\vartheta_{R1}}\right) \\ &= \frac{\vartheta_{T1} \pm \vartheta_{R1}}{2}\end{aligned} \tag{48}$$

$$\begin{aligned}&\frac{\partial(R_{T1} + R_{R1} - R_{T2} - R_{R2})}{\partial\bar{\vartheta}} \\ &= \frac{\partial(R_{T1} + R_{R1} - R_{T2} - R_{R2})}{\partial x}\frac{\partial x}{\partial\bar{\vartheta}} = \eta_x\frac{\partial x}{\partial\bar{\vartheta}}\end{aligned} \tag{49}$$

$$\frac{\partial z}{\bar{r}\partial\bar{\vartheta}} = \sin\bar{\vartheta}, \quad \frac{\bar{r}\partial\bar{\vartheta}}{\partial x} = \cos\bar{\vartheta} \tag{50}$$

with $\bar{r}$ being the curvature radius of the equirange line. By using (49) and (50) in (47), we get

$$\begin{aligned}\frac{\partial\Phi}{\partial z} &= \frac{2\pi}{\lambda}\eta_x\frac{\partial x}{\partial\bar{\vartheta}}\frac{\partial\bar{\vartheta}}{\partial z} \\ &= \frac{2\pi}{\lambda}\left(\frac{\cos\vartheta_{T1}B_{T\perp}}{r_{T1}} \pm \frac{\cos\vartheta_{R1}B_{R\perp}}{r_{R1}}\right)\frac{1}{\sin\bar{\vartheta}\cos\bar{\vartheta}}.\end{aligned} \tag{51}$$

This equation shows that if (45) is satisfied, then $\partial\Phi/\partial z = 0$, and there is no phase sensitivity to topography. Therefore, (45) provides the ideal condition for bistatic differential SAR interferometry.

It can be also noted that (51) in the monostatic repeat-pass case reduces to the well-known result

$$\frac{\partial\Phi}{\partial z} = \frac{4\pi}{\lambda}\frac{B_\perp}{r_1\sin\vartheta_1}. \tag{52}$$

Finally, we note that in the coplanar geometry, the case of single transmitter can be easily recovered by replacing $B_{T\perp} = 0$ in (40), (41), and (51), whereas (42) holds as it is.

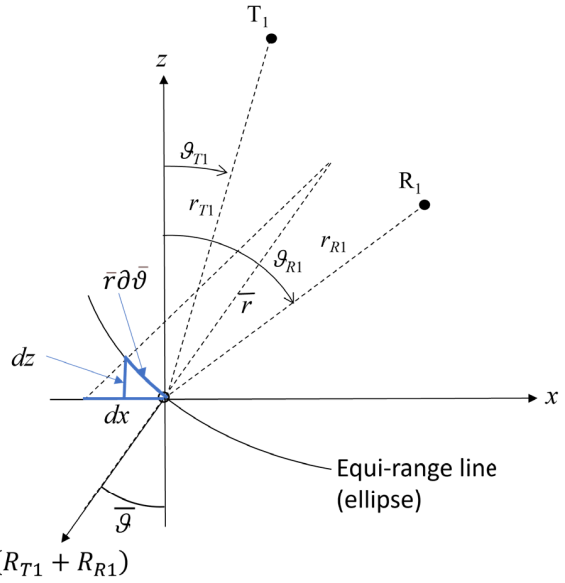

Fig. 3. Geometry for the evaluation of the phase sensitivity to topography. An equirange line is highlighted. Its normal unit vector is the gradient of $R_{T1} + R_{R1}$, whose x and z components are u_x and $-u_z$, respectively.

TABLE I
BISTATIC SAR SYSTEM PARAMETERS

Parameter	Symbol	Value
Wavelength	λ	3 cm
Transmitter T1 height	z_{T1}	620 km
T1 look angle	ϑ_{T1}	30°
T1 azimuth angle	φ_{T1}	0°
Azimuth baselines	B_{Taz}, B_{Raz}	0
Receiver R1 height	z_{R1}	620 km
Semi-resolution along x	A_x	5 m
Semi-resolution along y	A_y	5 m
Transmitter perpendicular baseline	$B_{T\perp}$	400 m (Scenarios A, B, D) 0 m (Scenarios C, E)
R1 look angle	ϑ_{R1}	[15°, 45°, 60°] (Scenarios A, B, C) 30° (Scenario D) Set according to (55) (Scenario E)
R1 azimuth angle	φ_{R1}	0° (Scenario A) 180° (Scenario B) [5°, 30°, 60°] (Scenario D) Set according to (56) (Scenario E)

IV. NUMERICAL RESULTS

In this section, we present and discuss some numerical results of the correlation coefficient derived in Section II. We considered the X-band bistatic SAR system described in Table I and analyzed four different scenarios that might be relevant in practical situations and that differ for the bistatic-imaging configuration.

1) *Scenario A:* Coplanar geometry, as described in Section III-B, in a backward scattering configuration, that is, $\varphi_{R1} = 0$, see Fig. 2(a).
2) *Scenario B:* Coplanar geometry in forward-scattering configuration, that is, $\varphi_{R1} = \pi$, see Fig. 2(b).
3) *Scenario C:* Noncoplanar geometry with a single transmitter, see Fig. 4.

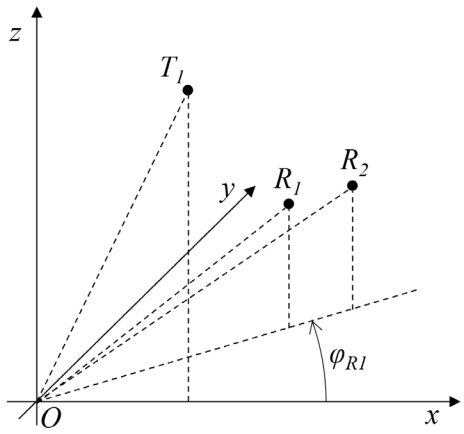

Fig. 4. Noncoplanar geometry with a single transmitter (Scenario C).

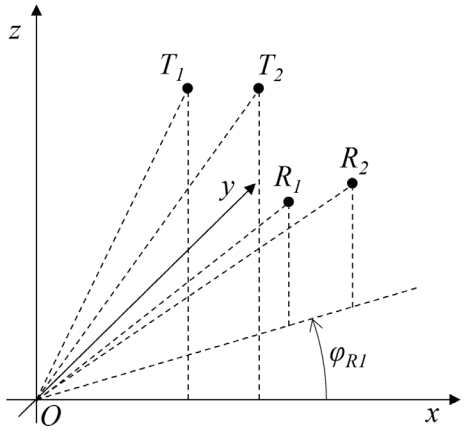

Fig. 5. Noncoplanar geometry with two transmitters (Scenario D).

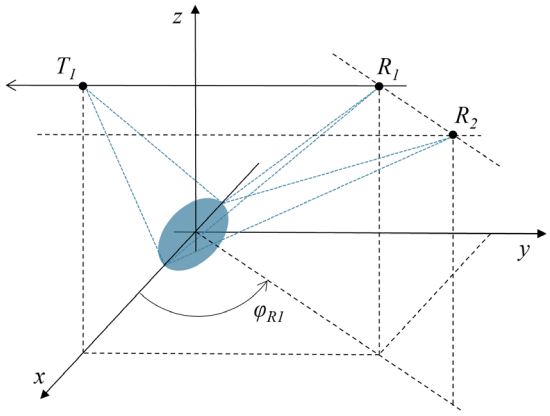

Fig. 6. Along-track bistatic geometry with a single transmitter (Scenario E).

4) *Scenario D:* Noncoplanar geometry with two transmitters, see Fig. 5.
5) *Scenario E:* Along-track bistatic geometry with a single transmitter, see Fig. 6. In this configuration, both the transmitter and the receiver $R1$ are assumed to move along the same trajectory that is parallel to the y-axis.

All such cases have been defined according to the simplifying assumptions of (34), namely $\varphi_{T1} = 0$, $\sigma \ll A_x$, and $B_{Taz} = B_{Raz} = 0$. Accordingly, the simulation results presented in this section are independent upon the surface roughness, as discussed in Section III. Moreover, apart from Scenarios C and E, all other scenarios consider a nonnull transmitter perpendicular baseline, that is, two separated transmitters or a single transmitter in a repeat-pass mode are considered.

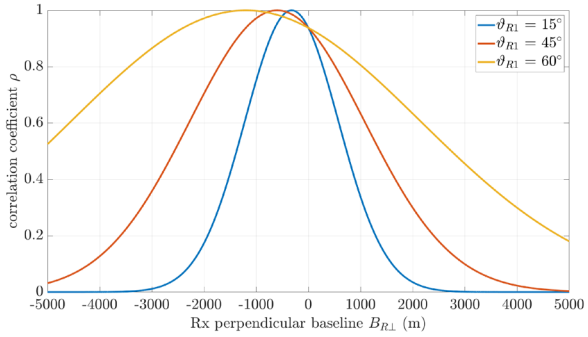

Fig. 7. Correlation coefficient in Scenario A (coplanar, backward) as a function of the receiver perpendicular baseline $B_{R\perp}$ for different R1 look angles.

It is also worth mentioning that the imaging configuration of Scenarios A and E are of particular practical interest, as they are considered in some planned or proposed passive bi- and multistatic SAR systems, namely, PLT-1/CSG (for which both scenarios are of interest) [11] and SESAME (for which Scenario E is of interest) [8].

Numerical results for the five scenarios are shown in Figs. 7–11, where the correlation coefficient is reported as a function of the main bistatic system geometry parameters.

In all the scenarios, the rate of change of the correlation coefficient with the receiver baseline is larger with smaller $R1$ look angle ϑ_{R1}.

In the coplanar geometries (Scenarios A and B) it can be seen that, as stated in Section III-B and according to (45), unitary correlation coefficient can be achieved with nonnull orthogonal baselines. More specifically, the value of the receiver orthogonal baseline for which this happens increases (in absolute value) with increasing $R1$ look angle, fixed all other system parameters, reaching absolute values slightly larger than 1 km for the considered bistatic system.

From a practical viewpoint, it is worth noting that this unitary-correlation receiver orthogonal baseline has the same (opposite) sign of the transmitter orthogonal one in the coplanar forward (backward) configuration. In other words, the lower receiver must collect the signal transmitted by the lower (higher) transmitter in the co-planar forward (backward) geometry. By inspecting Figs. 7 and 8, it is also evident that a symmetry does exist. Indeed, according to (34), the correlation coefficient is invariant with respect to the formal changes $\varphi_{R1} \to \pi - \varphi_{R1}$ and $B_{R\perp} \to -B_{R\perp}$. Similarly, no changes take place by replacing φ_{R1} with its opposite, that is, under the hypothesis of (34) the sign of φ_{R1} is unessential, which is intuitive, assumed the isotropy of the scattering surface.

Let us move to the noncoplanar geometries, that is, Scenarios C and D. As noted in Section II, for the considered system parameters, in Scenario C, the correlation coefficient is

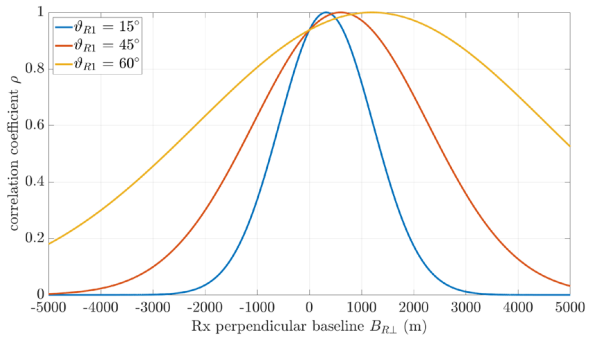

Fig. 8. Correlation coefficient in Scenario B (coplanar, forward) as a function of the receiver perpendicular baseline $B_{R\perp}$ for different R1 look angles.

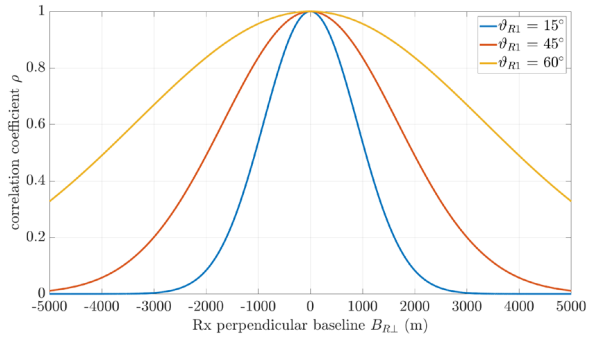

Fig. 9. Correlation coefficient in Scenario C (noncoplanar with a single transmitter) as a function of the receiver perpendicular baseline $B_{R\perp}$ for different R1 look angles.

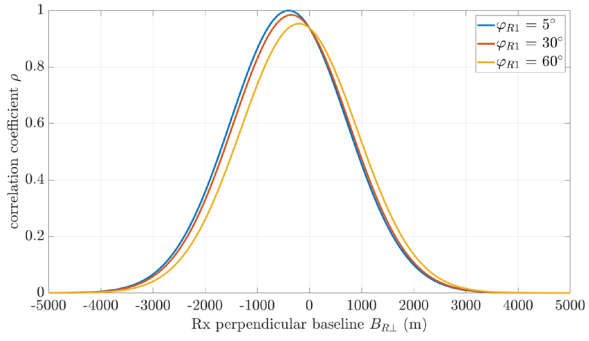

Fig. 10. Correlation coefficient in Scenario D (noncoplanar with two transmitters) as a function of the receiver perpendicular baseline $B_{R\perp}$ for different R1 azimuth angles.

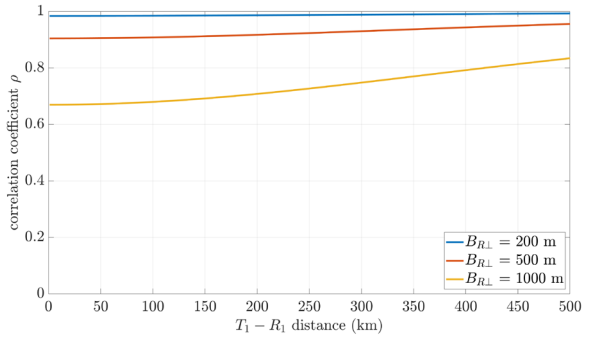

Fig. 11. Correlation coefficient in Scenario E (along-track bistatic geometry with a single transmitter) as a function of the distance between the transmitter T_1 and the receiver R_1 for different receiver perpendicular baselines $B_{R\perp}$.

independent of the $R1$ azimuth angle φ_{R1}. Additionally, as it would be expected, in the presence of a single transmitter, exchanging the receivers does not change the correlation between the received fields. This reflects in the evenness of the correlation coefficient with respect to the receiver orthogonal baseline $B_{R\perp}$ and, accordingly, in the maximum correlation achieved for null baseline, $B_{R\perp} = 0$, see Fig. 9.

The case of two separated transmitters (Scenario D), that is, nonnull transmitter orthogonal baseline $B_{T\perp}$, is considered in Fig. 10, where we show the correlation coefficient for different $R1$ azimuth angles φ_{R1}, namely 5°, 30°, and 60°, which correspond to y-coordinates of $R1$ equal to 31.20, 178.98, and 310 km, respectively. As $T1$ and $R1$ share the same altitude and look angle in the considered imaging geometry, the y-coordinate of $R1$ approximately equals the distance between the receiver and the corresponding transmitter.

As for the coplanar scenarios, in the presence of two transmitters, the largest correlation coefficient is obtained with nonnull orthogonal receiver baseline. This maximum-correlation baseline decreases with increasing transmitter-to-receiver distance. However, for the considered system, the maximum correlation is slightly lower than one and decreases with increasing transmitter-to-receiver distance, as it would be expected. Indeed, under the hypotheses of (34), it can be shown that, if the additional hypothesis of equal system resolutions is along x and y, that is, $A_x = A_y = A$, holds, the receiver orthogonal baseline $B_{R\perp,\mathrm{mc}}$ that ensures the largest possible correlation coefficient can be expressed as

$$B_{R\perp,mc} = -B_{T\perp}\frac{r_{R1}}{r_{T1}}\frac{\cos\vartheta_{T1}}{\cos\vartheta_{R1}}\cos\varphi_{R1}. \tag{53}$$

The corresponding maximum correlation value is

$$\begin{aligned}\rho_{\max} &= \rho\left(B_{R\perp} = B_{R\perp,mc}\right)\\ &= \exp\left\{-\frac{k^2A^2}{4}\frac{\cos^2\vartheta_{T1}B_{T\perp}^2}{r_{T1}^2}\left(1-\cos^2\varphi_{R1}\right)\right\}.\end{aligned} \tag{54}$$

Equation (54) also demonstrates that a unitary correlation coefficient is achievable only in coplanar geometries, that is, for $\varphi_{R1} = 0, \pi$, while the maximum value of the correlation becomes smaller and smaller as φ_{R1} approaches $\pm\pi/2$. It should be also noted that the correlation between the received fields is much less dependent on the azimuth angle than on the look angle.

Finally, let us move to the along-track bistatic geometry (Scenario E, see Fig. 6). In this case, the $R1$ look and azimuth angles are set according to the along-track $T1$–$R1$ distance d_{T1R1} as follows:

$$\vartheta_{R1} = \tan^{-1}\left(\frac{\sqrt{d_{T1R1}^2 + (z_{T1}\tan\vartheta_{T1})^2}}{z_{T1}}\right) \tag{55}$$

$$\varphi_{R1} = \tan^{-1}\left(\frac{d_{T1R1}}{z_{T1}\tan\vartheta_{T1}}\right). \tag{56}$$

Fig. 11 shows the correlation coefficient as a function of d_{T1R1} for different receiver perpendicular baseline $B_{R\perp}$.

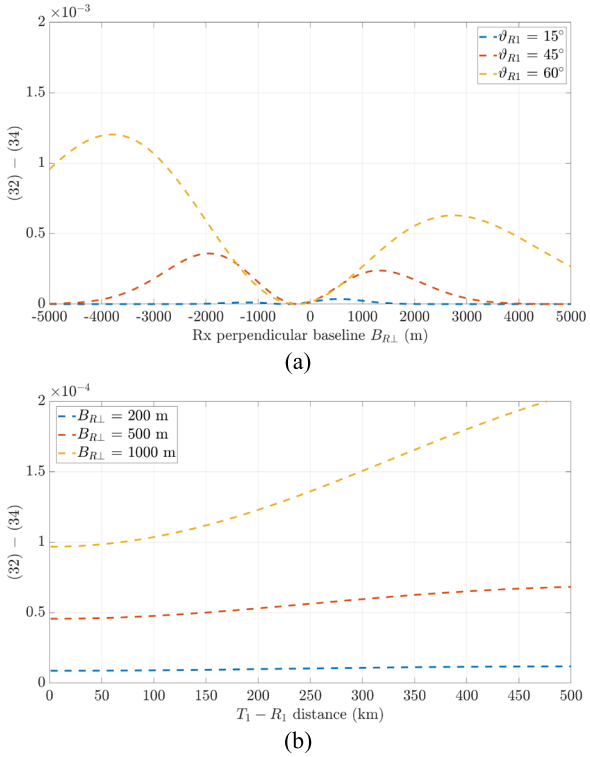

Fig. 12. Difference between the correlation coefficient evaluated according to (34) and (32) in (a) Scenario A and (b) Scenario E.

By recalling that in the considered geometry, the correlation coefficient is an even function of $B_{R\perp}$, see (34), we limit our analysis to positive baseline values. As it would be expected, the correlation coefficient improves with the $T1$–$R1$ distance regardless of the baseline, as the angular separation between the receivers decreases with increasing distance for a fixed baseline; analogously, the received fields are less and less correlated with increasing baseline. However, correlation values larger than 0.9 are obtained with receiver baseline up to 500 m, regardless of the $T1$–$R1$ distance.

A final comment about the reliability of using (34) instead of the more general formulation in (32) is in order. Fig. 12 shows the difference between the approximation in (34) and the full expression in (32) for the scenarios A [Fig. 12(a)] and E [Fig. 12(b)]. It can be seen that the error is lower than 1.5×10^{-3} regardless of the varying parameters in both cases.

V. Conclusion

In this article, we have presented a new analytical approach for the evaluation of the spatial correlation coefficient for a bistatic SAR interferometric system. The proposed methodology makes use of electromagnetic scattering models for bare soil surfaces which are modeled as normally distributed random rough surfaces. By adopting a quite general formulation of the scattering problem, we derived closed-form expressions of the spatial correlation at the receivers which are valid under both the KA and the SSA1, the latter exhibiting a much larger applicability with respect to the former.

To this end, we considered a very generic bistatic imaging geometry which includes two transmitters and two receivers. Specific imaging cases of practical interest, including coplanar and along-track bistatic geometries as well as well single-transmitter systems, were analyzed, and simplified expressions for both the correlation coefficient and the critical baseline were derived. In such configurations, numerical results for an X-band bistatic SAR system have been presented and discussed.

It has been found that, in the case of a single transmitter, as expected, the correlation coefficient decreases with increasing orthogonal baseline. Interestingly, in the case of two separate transmitters, it has been found that, in coplanar imaging geometries, a unitary correlation coefficient can be obtained with nonnull orthogonal baselines, while in out-of-plane, that is, noncoplanar, geometries, the maximum value of the correlation coefficient is slightly lower than unity and is achieved for a receiver orthogonal baseline which is proportional to the transmitter one.

The proposed models might be fruitfully exploited for the design and the analysis of bistatic SAR systems, such as SESAME and CSG/PLT-1, with a special emphasis on the performance analysis of interferometric applications. It is worth mentioning that, compared to numerical and experimental analyses, our analytical approach is flexible and allows for a fast evaluation of the correlation coefficient for any bistatic imaging configuration and natural scene, provided that surface scattering is the dominant contribution, and that KA or SSA-1 are applicable, such as in the presence of bare soil surfaces or scarcely to moderately vegetated areas. Indeed, both scattering theories ignore multiple scattering and do not provide reliable evaluations of the scattered field if surface scattering is not the dominant mechanisms, as in the case of dense vegetation and urban areas. However, it should be noted that InSAR application is of limited interest in the latter cases, as well as DInSAR is problematic in densely vegetated areas due to the low coherence. Additionally, the proposed analytical formulation provides physical insights into the scattering mechanisms ruling the correlation between the received fields.

Possible further research activities might focus on the adoption of more advanced surface models, such as those based on the fractal geometry and/or accounting for surface anisotropy, and electromagnetic scattering methods. Concerning this latter point, the adoption of two-scale models might unveil distinct impacts of microscopic and macroscopic roughness on the correlation, while polarimetric methods might enable the analysis of bistatic polarimetric interferometric SAR systems. Finally, it should be stressed here that a comprehensive validation of the proposed formulations cannot be undertaken so far, as neither the measurements nor the simulators of bistatic interferometric SAR products are available. Indeed, the obtained correspondence with the monostatic formulation is encouraging, despite not being sufficient. Accordingly, future research efforts should focus on proper validation activities using real-world bistatic interferometric SAR measurements as well as on the development of reliable numerical simulators of such products.

ACKNOWLEDGMENT

The authors are grateful to Dr.-Ing. Giovanni Paolo Blasone, Italian Space Agency, for his useful suggestions.

REFERENCES

[1] H. A. Zebker and R. M. Goldstein, "Topographic mapping from interferometric synthetic aperture radar observations," *J. Geophys. Res.*, vol. 91, no. B5, pp. 4993–4999, Apr. 1986.

[2] E. Rodriguez and J. M. Martin, "Theory and design of interferometric synthetic aperture radars," *IEE Proc. F Radar Signal Process.*, vol. 139, no. 2, pp. 147–159, Apr. 1992.

[3] A. K. Gabriel, R. M. Goldstein, and H. A. Zebker, "Mapping small elevation changes over large areas: Differential radar interferometry," *J. Geophys. Res., Solid Earth*, vol. 94, no. B7, pp. 9183–9191, Jul. 1989.

[4] A. Ferretti, C. Prati, and F. Rocca, "Permanent scatterers in SAR interferometry," *IEEE Trans. Geosci. Remote Sens.*, vol. 39, no. 1, pp. 8–20, Apr. 2001.

[5] P. Berardino, G. Fornaro, R. Lanari, and E. Sansosti, "A new algorithm for surface deformation monitoring based on small baseline differential SAR interferograms," *IEEE Trans. Geosci. Remote Sens.*, vol. 40, no. 11, pp. 2375–2383, Nov. 2002.

[6] R. Bamler, "The SRTM mission: A world-wide 30 m resolution DEM from SAR interferometry in 11 days," in *Photogrammetric Week*, vol. 1999, R. Fritsch R. Spiller, Ed., Heidelberg, Germany: Wichmann Verlag, 1999, pp. 145–154.

[7] M. Zink et al., "TanDEM-X: 10 years of formation flying bistatic SAR interferometry," *IEEE J. Sel. Topics Appl. Earth Observ. Remote Sens.*, vol. 14, pp. 3546–3565, 2021.

[8] P. López-Dekker et al., "Companion SAR constellations for single-pass interferometric applications: The SESAME mission," in *Proc. IEEE Int. Geosci. Remote Sens. Symp. (IGARSS)*, Fort Worth, TX, USA, Jul. 2017, pp. 119–122.

[9] S. Duque, P. Lopez-Dekker, and J. J. Mallorqui, "Single-pass bistatic SAR interferometry using fixed-receiver configurations: Theory and experimental validation," *IEEE Trans. Geosci. Remote Sens.*, vol. 48, no. 6, pp. 2740–2749, Jun. 2010.

[10] G. Farquharson et al., "The new capella space satellite generation: Acadia," in *Proc. IEEE Int. Geosci. Remote Sens. Symp.*, Pasadena, CA, USA, Jul. 2023, pp. 1513–1516.

[11] A. Renga et al., "Bistatic SAR techniques and products in a long baseline spaceborne scenario: Application to PLATiNO-1 mission," in *Proc. EUSAR*, Munich, Germany, 2024, pp. 884–888.

[12] H. A. Zebker and J. Villasenor, "Decorrelation in interferometric radar echoes," *IEEE Trans. Geosci. Remote Sens.*, vol. 30, no. 5, pp. 950–959, Sep. 1992.

[13] G. Franceschetti, A. Iodice, M. Migliaccio, and D. Riccio, "The effect of surface scattering on ifsar baseline decorrelation," *J. Electromagn. Waves Appl.*, vol. 11, no. 3, pp. 353–370, Jan. 1997.

[14] A. Ishimaru and J. S. Chen, "Scattering from very rough surfaces based on the modified second-order Kirchhoff approximation with angular and propagation shadowing," *J. Acoust. Soc. Amer.*, vol. 88, no. 4, pp. 1877–1883, Oct. 1990.

[15] M. E. Knotts, T. R. Michel, and K. A. O'Donnell, "Angular correlation functions of polarized intensities scattered from a one-dimensionally rough surface," *J. Opt. Soc. Amer. A, Opt. Image Sci.*, vol. 9, no. 10, pp. 1822–1831, 1992.

[16] T. R. Michel and K. A. O'Donnell, "Angular correlation functions of amplitudes scattered from a one-dimensional, perfectly conduction rough surface," *J. Opt. Soc. Amer. A, Opt. Image Sci.*, vol. 9, no. 8, pp. 1374–1384, 1992.

[17] C. T. C. Le, Y. Kuga, and A. Ishimaru, "Angular correlation function based on the second-order Kirchhoff approximation and comparison with experiments," *J. Opt. Soc. Amer. A, Opt. Image Sci.*, vol. 13, no. 5, pp. 1057–1067, May 1996.

[18] G. Zhang, L. Tsang, and Y. Kuga, "Studies of the angular correlation function of scattering by random rough surfaces with and without a buried object," *IEEE Trans. Geosci. Remote Sens.*, vol. 35, no. 2, pp. 444–453, Mar. 1997.

[19] G. Di Martino, A. Di Simone, and A. Iodice, "An analytical formulation of the correlation of GNSS-R signals," *IEEE Trans. Geosci. Remote Sens.*, vol. 60, 2022, Art. no. 2005913.

[20] G. Di Martino, A. Di Simone, and A. Iodice, "A novel analytical formulation of the correlation of GNSS-R signals scattered by a natural fractal surface," *IEEE Geosci. Remote Sens. Lett.*, vol. 21, pp. 1–5, 2024.

[21] G. Di Martino, A. Di Simone, and A. Iodice, "An analytical formulation for the correlation of surface-scattered fields at two bistatic radar receivers," in *Proc. IEEE Int. Geosci. Remote Sens. Symp.*, Kuala Lumpur, Malaysia, Jul. 2022, pp. 4969–4972.

[22] F. T. Ulaby, R. K. Moore, and A. K. Fung, *Microwave Remote Sensing*, vol. 2. Reading, MA, USA: Artech-House, 1982.

[23] A. Voronovich, "Small-slope approximation for electromagnetic wave scattering at a rough interface of two dielectric half-spaces," *Waves Random Media*, vol. 4, no. 3, pp. 337–367, Jul. 1994.

[24] A. Papoulis, *Probability, Random Variables, and Stochastic Processes*, 3, Ed., New York, NY, USA: McGraw-Hill, 1991.

Gerardo Di Martino (Senior Member, IEEE) was born in Naples, Italy, in 1979. He received the Laurea degree (cum laude) in telecommunication engineering and the Ph.D. degree in electronic and telecommunication engineering from the University Federico II, Naples, in 2005 and 2009, respectively.

From 2014 to 2015, he was with Italian National Consortium for Telecommunications (CNIT), Naples, andwith the Regional Center Information Communication Technology (CeRICT), Naples, in 2016. He is currently an Associate Professor of electromagnetic fields with the Department of Electrical Engineering and Information Technology, University of Naples Federico II. His research interests include microwave remote sensing and electromagnetics, with focus on electromagnetic scattering from natural surfaces and urban areas, synthetic aperture radar (SAR) signal processing and simulation, information retrieval from SAR data, and electromagnetic propagation in urban areas.

Prof. Di Martino is an Ex-Officio Member of IEEE GRSS Administrative Committee (AdCom). He is a Lead Editor of IEEE GEOSCIENCE AND REMOTE SENSING SOCIETY (GRSS) Section within IEEE ACCESS and an Associate Editor of IEEE JOURNAL OF SELECTED TOPICS ON APPLIED EARTH OBSERVATIONS AND REMOTE SENSING.

Alessio Di Simone (Member, IEEE) was born in Torre del Greco, Italy, in 1989. He received the B.Sc. and M.Sc. Laurea degrees (cum laude) in telecommunication engineering and the Ph.D. degree in information technology and electrical engineering from the University of Naples Federico II, Naples, Italy, in 2011, 2013, and 2017, respectively.

In 2016, he joined the Universitat Politècnica de Catalunya, Barcelona, Spain, as a Visiting Researcher. In 2017, 2018, and 2023, he was a Visiting Researcher with the NATO Science and Technology Organization, Centre for Maritime Research and Experimentation (CMRE), La Spezia, Italy. From 2017 to 2021, he was a Research Fellow with the Department of Electrical Engineering and Information Technology, University of Naples Federico II, where he has been an Assistant Professor of electromagnetic fields, since 2022. His main research interests are in the field of microwave remote sensing and electromagnetics including modeling of the electromagnetic scattering from natural surfaces, urban areas, and artificial targets, and simulation and processing of synthetic aperture radar (SAR) and global navigation satellite system reflectometry (GNSS-R) data.

Dr. Di Simone received the Prize for the Best Master Thesis in Remote Sensing by the IEEE South Italy Geoscience and Remote Sensing Chapter in 2015 and the 2022 Best Young Researcher in Oceanic Engineering Award from the IEEE Oceanic Engineering Italy Chapter. In 2023, he was awarded with the National Scientific Qualification as Associate Professor of Electromagnetic Fields.

Antonio Iodice (Senior Member, IEEE) was born in Naples, Italy, in 1968. He received the Laurea degree (cum laude) in electronic engineering and the Ph.D. degree in electronic engineering and computer science from the University of Naples "Federico II," Naples, in 1993 and 1999, respectively.

In 1995, he was with the Research Institute for Electromagnetism and Electronic Components of the Italian National Council of Research (IRECE-CNR), Naples, and from 1999 to 2000 with Telespazio S.p.A., Rome, Italy. He was at the University of Naples "Federico II" as a Research Scientist, from 2000 to 2004 and as a Professor of electromagnetics, from 2005 to 2018. He is currently a Full Professor of electromagnetics at the Department of Electrical Engineering and Information Technology, University of Naples "Federico II," where he is also the Coordinator of the B.S. and M.S. degree programs in telecommunications and digital media engineering. He has been involved as a Principal Investigator or Co-Investigator in several projects funded by European Union (EU), Italian Space Agency (ASI), Italian Ministry of Education and Research (MIUR), Campania Regional Government, and private companies. He has authored or coauthored two books and more than 350 papers, of which over 100 were published in refereed journals. His main research interests are in the field of microwave remote sensing and electromagnetics: modelling of electromagnetic scattering from natural surfaces and urban areas, simulation and processing of synthetic aperture radar (SAR) signals, and electromagnetic propagation in urban areas.

Prof. Iodice received the "2009 Sergei A. Schelkunoff Transactions Prize Paper Award" from the IEEE Antennas and Propagation Society, for the best paper published in 2008 on IEEE TRANSACTIONS ON ANTENNAS AND PROPAGATION. He was recognized by the IEEE Geoscience and Remote Sensing Society as a 2015 Best Reviewer of IEEE TRANSACTIONS ON GEOSCIENCE AND REMOTE SENSING. He is the Past Chair of the IEEE Geoscience and Remote Sensing South Italy Chapter and a Senior Member of the URSI.

Daniele Riccio (Fellow, IEEE) was born in Naples, Italy. He received the Laurea degree (cum laude) in electronic engineering from the University of Naples Federico II, Naples, in 1989.

His career has been developing at the University of Naples Federico II, where he is a Full Professor of electromagnetic fields with the Department of Electrical Engineering and Information Technology. He was a Research Scientist with Italian National Research Council from 1989 to 1994, a Guest Scientist with German Aerospace Centre (DLR), Germany from 1994 to 1995, and a Research Affiliate to NASA, Washington, DC, USA from 2010 to 2018. He lectured abroad (Spain, Czech Republic) in Ph.D. Schools. He is a member of the Cassini Radar Science Team and Italian Space Agency Platino-1 Mission Advisory Group. At the University of Naples Federico II, he is a Rector Delegate for Ph.D. Schools, and coordinates the Ph.D., School in information and communication technology for health. He is a Board Member for the Ph.D. Programme on Space at the Scuola Superiore Meridionale, Naples. He is a member of the Board of Directors for the RESTART Foundation in Charge of the Telecommunications of the Future PNRR Programme. He is an Athenaeum Representative with Italian Society of Electromagnetism (SIEm), where he was a member of the Board of Directors appointed with a Secretary role. He is the Director of the National Laboratory on Multimedia Communications. He has authored four books and 500 scientific papers. His research interests include electromagnetic theory, remote sensing, electromagnetic scattering from complex media and surfaces, synthetic aperture radar techniques, application of fractal geometry to remote sensing, and propagation of electromagnetic fields for wireless communication networks planning.

Prof. Riccio was a recipient of the 2009 Sergei A. Schelkunoff Transactions Prize Paper Award for the Best Paper Published in 2008 on IEEE TRANSACTIONS ON ANTENNAS AND PROPAGATION. He has been the General Chair of the 5G International Ph.D. School, since 2018. He is an Associate Editor for some journals on *Remote Sensing*.

Giuseppe Ruello (Senior Member, IEEE) received the Laurea degree (cum laude) in telecommunication engineering and the Ph.D. degree in information engineering from the University of Naples Federico II, Naples, Italy, in 1999 and 2003, respectively.

He is an Associate Professor at the Department of Electrical and Information Technology Engineering, University of Naples Federico II. In 2019, he was appointed as a Fulbright Scholar at the Department of Radiology, New York University, New York, NY, USA. In 2002, 2004, and 2005, he was a Visiting Scientist with the Department of Signal Theory and Communications, Universitat Politecnica de Catalunya of Barcelona, Barcelona, Spain. He has authored or co-authored more than 200 publications, including more than 50 articles in peer-reviewed journals. His main research interests include synthetic aperture radar (SAR) remote sensing, modelling of electromagnetic scattering from natural surfaces, fractal models, SAR raw signal simulation, modelling of electromagnetic field propagation in urban environment, and radiofrequency field modelling in magnetic resonance applications.

Open Access funding provided by 'Università degli Studi di Napoli "Federico II"' within the CRUI CARE Agreement